Paper 85

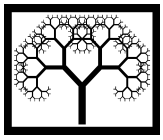

Proceedings of the Eighth International Conference on Engineering Computational Technology, B.H.V. Topping, (Editor), Civil-Comp Press, Stirlingshire, Scotland

Magnetohydrodynamic Flow of a Liquid Metal in a Curved Circular Duct subject to the Effect of an External Magnetic Field

P.A. Bakalis, P.M. Hatzikonstantinou and P. Vafeas
Department of Engineering Sciences
Division of Applied Mathematics & Mechanics
University of Patras, Greece

Abstract

The fully developed magnetohydrodynamic (MHD) flow of a liquid metal in a curved circular pipe is numerically studied in the present paper, under the effect of an external applied transverse magnetic field. The complementary variational principle (CVP) numerical method is used for the coupling of the continuity and the Navier-Stokes equations and a hybrid formulation is used for the implementation of the electromagnetic variables. The main interest here is to determine the redistribution of the velocity for different parameters of curvature and Hartmann number.

Keywords: magnetohydrodynamics, curved duct, numerical analysis, complementary variational principle method.

1 Introduction

In magnetohydrodynamics (MHD), the flow of a liquid metal is influenced by an external magnetic field. This mutual interaction arises partially as a result of the laws of Faraday and Ampère and partially because of the Lorentz force. The content of the present paper is focused on the MHD flow of a liquid metal within a circular duct with moderate curvature κ and moderate Hartmann numbers. Many designs of liquid metal flows, such as fusion reactors or power generation, involve curved circular ducts.

Only few theoretical and experimental works on curved MHD flows have been published up to today. Kobayashi [1] studied the effect of a perpendicular external magnetic field on the secondary vortex flow of a curved channel, for small Hartmann numbers, showing that the primary flow is stabilized by the magnetic field effect. Sudou and Tomita [2] performed a theoretical and experimental analysis for the flow of a liquid metal in a curved circular channel for small Hartmann

numbers and small curvatures. Their results show that as the magnetic field increases the secondary flow is suppressed by the magnetic field. The laminar MHD flow in a rectangular curved channel is studied by Tabeling and Chabrerie [3] at intermediate Hartmann numbers, using an analytical perturbation method. Issacci *et. al* [4] studied analytically the MHD flow in a circular channel for small and intermediate Hartmann numbers and small curvatures.

In the case of the fully developed MHD flow on straight ducts, several studies have been carried out for conducting or insulated channels using the finite-difference or the finite element method, such as [5] and [6].

The fully developed magnetohydrodynamic (MHD) flow of a liquid metal in a curved circular channel, under an external transverse magnetic field is studied numerically for the first time in the present paper. Results are presented for various curvatures κ=0, 0.05, 0.1, 0.2 and for Hartmann number in the range $0 \le Ha \le 200$. The computational method that was used to couple the Navier-Stokes and continuity equation was the CVP computational method, which has been developed by P. Hatzikonstantinou *et al* [7, 8]. The CVP method has already been validated and tested in several 2D and 3D hydrodynamic and MHD channel flows, such as [9] and [10].

For the implementation of the electromagnetic quantities, a hybrid formulation will be used, that computes the axial component of the electric current density from the Ohm's law and the transverse components of the electric current density from the Ampere's law [11].

2 Problem Formulation

The MHD flow of an incompressible electrically conducting fluid, under the action of an external magnetic field $\vec{B}_o$ is governed by the following set of non-dimensional equations:

Momentum equation: $\partial\vec{V}/_{\partial t} + (\vec{V}.\vec{\nabla})\vec{V} = -\vec{\nabla}P + 1/_{Re}.\Delta\vec{V} + Ha^2/_{Re}.\vec{J}\times\vec{B}$

Continuity equation: $\vec{\nabla}\vec{V} = 0$

Transport of magnetic induction: $\partial\vec{B}/_{\partial t} + (\vec{V}.\vec{\nabla})\vec{B} = 1/_{R_m}.\Delta\vec{B} + (\vec{B}.\vec{\nabla})\vec{V}$

Divergence free equation for magnetic field: $\vec{\nabla}\vec{B} = 0$

Ohm's law: $\vec{J} = -\vec{\nabla}\Phi + \vec{V}\times\vec{B}_o$

Amperes law: $\vec{J} = 1/_{R_m}\,\vec{\nabla}\times\vec{B}_i$

Divergence free equation for the electric current density: $\vec{\nabla}\mathrm{J} = 0$

where $\vec{V}$ is the velocity, P is the pressure, $\vec{B}_o$ and $\vec{B}_i$ are, respectively, the external and the induced magnetic field, $\vec{J}$ is the current density, and Φ is the potential of the electric field.

The above equations became dimensionless using the following scales

$$t = \frac{t'V_0}{R'}, r = \frac{r'}{R'}, z = \frac{z'}{R'}, R_c = \frac{R_c'}{R'}, \vec{V} = \frac{\vec{V}'}{V_0}, P = \frac{P'}{\rho V_0^2}, \vec{B} = \frac{\vec{B}'}{B_0}, \vec{J} = \frac{\vec{J}'}{\sigma V_0 B_0}$$

and the following parameters: the Reynolds number $\mathrm{Re} = V_0 R/v$, the Hartmann number $Ha = \sqrt{\sigma/\rho\nu} B_0 R$ and the magnetic Reynolds number $\mathrm{R_m} = \mu\sigma \mathrm{V_o L}$.

We consider a curved circular duct with radius R and radius of curvature R_c, with respect to a Cartesian reference system (x,y,z) of Figure 1, the coordinates of which are transformed to a toroidal-poloidal coordinate system (r,θ,z).

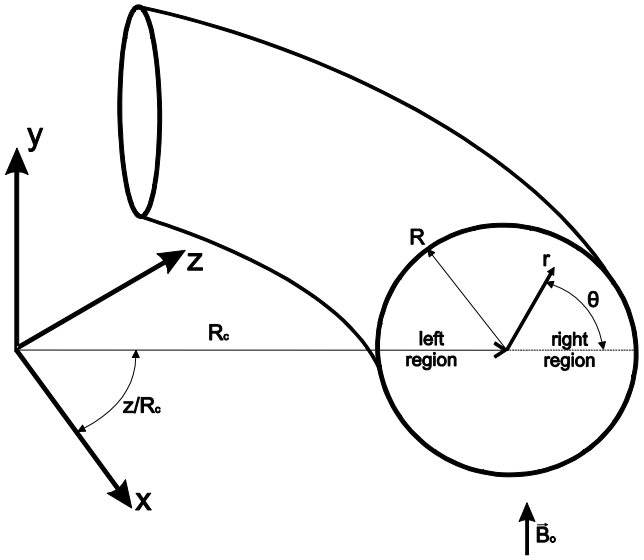

Figure 1. Toroidal-Poloidal coordinate system

In the laminar fully developed incompressible flow, the velocity $\vec{V} = \mathrm{u}\hat{e}_r + \mathrm{v}\hat{e}_\theta + \mathrm{w}\hat{e}_z$ and all the other variables are regarded as functions of r and θ only. The pressure gradient varies only along the cross section of the duct, while it is constant along the axial direction. Thus, the pressure splits into two terms $P = p_a(z) + p(r,\theta)$, where the pressure gradient in the axial direction $p_{a,z}(z) = \partial P/\partial z = \partial p_a/\partial z$ is computed by the mass conservation equation.

The flow is subjected to an external constant magnetic field $\vec{B}_o = B_o\hat{j} = B_{or}\hat{e}_r + B_{o\theta}\hat{e}_\theta = \sin\theta\hat{e}_r + cos\theta\hat{e}_\theta$, and an induced axial magnetic field $\vec{B}_i = b\hat{e}_z$. The total magnetic field is given by $\vec{B} = \vec{B}_o + \vec{B}_i$ and the produced

total electric current density is $\vec{J} = J_r\hat{e}_r + J_\theta\hat{e}_\theta + J_z\hat{e}_z$. The term $I = 1/(1+\kappa r cos\theta)$ is introduced, where $\kappa = 1/R_c$ is the curvature.

Hence the governing equations of the fully developed MHD flow of a liquid metal in toroidal-poloidal coordinates, take the following form

Continuity equation

$$\frac{\partial u}{\partial r} + \frac{u}{r} + \frac{1}{r}\frac{\partial v}{\partial \theta} + \kappa I(ucos\theta - vsin\theta) = 0 \qquad (1)$$

Navier Stokes equations at r-direction,

$$\frac{\partial u}{\partial t} + u\frac{\partial u}{\partial r} + \frac{v}{r}\frac{\partial u}{\partial \theta} - \frac{v^2}{r} - \kappa I w^2 cos\theta = -\frac{\partial P}{\partial r} + \frac{1}{Re}\left[\begin{array}{c}\frac{\partial^2 u}{\partial r^2} + \left(\frac{1}{r} + \kappa I cos\theta\right)\frac{\partial u}{\partial r} + \frac{1}{r^2}\frac{\partial^2 u}{\partial \theta^2} - \kappa I\frac{sin\theta}{r}\left(\frac{\partial u}{\partial \theta} - v\right) \\ -\frac{2}{r^2}\frac{\partial v}{\partial \varphi} - \frac{u}{r^2} + (\kappa I)^2(vsin\theta - ucos\theta)cos\theta\end{array}\right] + \frac{Ha^2}{Re}[J_\theta b - J_z B_{o\theta}] \qquad (2)$$

at θ-direction,

$$\frac{\partial v}{\partial t} + u\frac{\partial v}{\partial r} + \frac{v}{r}\frac{\partial v}{\partial \theta} + \frac{uv}{r} + \kappa I w^2 sin\theta = -\frac{1}{r}\frac{\partial P}{\partial \theta} + \frac{1}{Re}\left[\begin{array}{c}\frac{\partial^2 v}{\partial r^2} + \left(\frac{1}{r} + \kappa I cos\theta\right)\frac{\partial v}{\partial r} + \frac{1}{r^2}\frac{\partial^2 v}{\partial \theta^2} - \kappa I\frac{sin\theta}{r}\left(\frac{\partial v}{\partial \theta} + u\right) \\ +\frac{2}{r^2}\frac{\partial u}{\partial \theta} - \frac{v}{r^2} - (\kappa I)^2(vsin\theta - ucos\theta)sin\theta\end{array}\right] + \frac{Ha^2}{Re}[J_z B_{or} - J_r b] \qquad (3)$$

and at z-direction

$$\frac{\partial w}{\partial t} + u\frac{\partial w}{\partial r} + \frac{v}{r}\frac{\partial w}{\partial \theta} + \kappa I w(ucos\theta - vsin\theta) = -I\frac{\partial P}{\partial z} + \frac{1}{Re}\left[\frac{\partial^2 w}{\partial r^2} + \left(\frac{1}{r} + \kappa I cos\theta\right)\frac{\partial w}{\partial r} + \frac{1}{r^2}\frac{\partial^2 v}{\partial \theta^2} - \kappa I\frac{sin\theta}{r}\frac{\partial w}{\partial \theta} - (\kappa I)^2\right] + \frac{Ha^2}{Re}[J_r B_{o\theta} - J_\theta B_{or}] \qquad (4)$$

Axial magnetic field induction equation

$$\frac{\partial b}{\partial t} + u\frac{\partial b}{\partial r} + \frac{v}{r}\frac{\partial b}{\partial \theta} = \frac{1}{R_m}\left[\frac{\partial^2 b}{\partial r^2} + \left(\frac{1}{r} + \kappa I cos\theta\right)\frac{\partial b}{\partial r} + \frac{1}{r^2}\frac{\partial^2 b}{\partial \theta^2} - \kappa I\frac{sin\theta}{r}\frac{\partial b}{\partial \theta} - (\kappa I)^2 b\right]$$

$$+B_{or}\frac{\partial w}{\partial r}+\frac{B_{o\theta}}{r}\frac{\partial w}{\partial \theta}-\kappa Ib(vsin\theta-ucos\theta)+\kappa Iw\left(B_{o\theta}sin\theta-B_{o\_r}cos\theta\right) \quad (5)$$

The axial component of the electric current density J_z is computed by the Ohm's law and the transverse components $\vec{J}_t=(J_r,J_\theta)$ from the Ampere's law and thus we have:

$$J_z=uB_{o\theta}-vB_{or} \quad (6)$$

$$J_r=\frac{1}{R_m}\left[\frac{1}{r}\frac{\partial b}{\partial \theta}-\kappa Ibsin\theta\right] \text{ and } J_\theta=-\frac{1}{R_m}\left[\frac{\partial b}{\partial r}+\kappa Ibcos\theta\right] \quad (7)$$

The dimensionless radius of the circular pipe is R=1.0. No slip conditions are assumed for the walls, so that $u = v = w = 0$ for $r=R$. At the electrically insulating wall the magnetic field is $\vec{B}\big|_{wall}=\vec{B}_o\big|_{wall}$.

3 Computational Methodology – Numerical accuracy

The CVP numerical variational method will be used for the coupling of the continuity and the Navier-Stokes equation. The CVP method in addition to the continuity, momentum, and pressure equations involves an additional set of variational representations of the continuity and pressure equations. It has several advantages as it uses a non-staggered grid for the primitive variables and it generally does not require relaxation parameters. Moreover, the correction equations are expressed in vector form and they are not produced through manipulation of the discretized governing equations, which is the case for the pressure-linked and other numerical schemes. Thus, the transformation of the involved equations to non-Cartesian or generalized coordinate systems is relatively simple. The CVP method characteristics (extreme accuracy, robustness, easy convergence and easy implementation to complex geometries) make it unique for MHD applications. The implementation of the CVP method is analytically presented in [9].

Non-uniform stretched meshes will be used in order to compute accurately the MHD boundary layers near the walls, and particularly the Hartmann, and side layers, which are respectively vertical and parallel to the magnetic field. Thus, special attention should be paid for the regions near the cylinder wall, where thin velocity and electric current layers are formulated due to the effect of the magnetic field.

To refine the mesh near the walls, the following transformation for the r-coordinate is used

$$r_i=R\frac{(2a+b)\left(\frac{b+1}{b-1}\right)^{\frac{\bar{r}_i-a}{1-a}}+2a-b}{(2a+1)\left[\left(\frac{b+1}{b-1}\right)^{\frac{\bar{r}_i-a}{1-a}}+1\right]}$$, where a=0.2, $b=\sqrt{\frac{\sqrt{Ha}}{\sqrt{Ha}-1}}$ and i=1,2,...

With this formula, the mesh $s(\overline{r_i})$ can be transformed can be transformed into a refined mesh $s(r_i)$. Since a=0.2, the mesh will be more refined near the wall of the cylinder. The stretching parameter b is related with the Hartmann number, because as the Hartmann number increases, the layers decrease in thickness.

The computed data are visualized with the open source visualization software ParaView, using the Visualization Toolkit format (VTK) as the data processing and rendering engine.

The overall computation finishes when the following convergence criterion for the velocity components is achieved for two sequential time steps

$$\left| \frac{\psi_{i,j}^{n+1} - \psi_{i,j}^{n}}{\psi_{i,j}^{n+1}} \right| < \varepsilon = 10^{-5}$$

where $\psi_{i,j} = u_{r(i,j)}$, $u_{\theta(i,j)}$, $u_{z(i,j)}$, $T_{(i,j)}$ and n represents the iteration number.

4 Results-Discussion

The magnetohydrodynamic flow of a liquid metal in a curved circular pipe is studied for Re=100, R_m=0.001, $0 \leq Ha \leq 200$ and $0 \leq \kappa \leq 0.2$. The results are illustrated in order to demonstrate the effect of the curvature and the magnetic field on the velocity distribution.

The effect of the centrifugal force on the axial velocity is presented in Figure 2 for Ha = 0 and κ = 0, 0.05, 0.10 and 0.20. In the case of a straight duct (κ = 0) the axial velocity develops to an axisymmetric parabolic profile with the maximum value of the axial velocity to be located at the center of the pipe. As the curvature increases, the peak of the axial velocity profile is shifted to the right region of the cylinder due to the effect of the centrifugal forces and the maximum value of the axial velocity decreases.

In Figure 3 the effect of the magnetic field on the axial velocity distribution is shown for Ha=10 and for κ = 0, 0.05, 0.10 and 0.20. As the curvature increases, the electromagnetic Lorentz force which is generated due to the effect of the external magnetic field tends to shift the peak of the axial velocity to the left region of the cylinder in contrast to the effect of the centrifugal force which shifts the axial velocity to the right region of the cylinder. In the case of Ha=10 the balance between the electromagnetic force and the centrifugal force is almost zero and the distribution of the axial velocity does not significantly change as the curvature increases. The effect of the external magnetic field flattens the axial velocity profile in a direction parallel to the magnetic field and thin Hartmann boundary layers begin to formulate near the top and bottom sides of the cylinder, as a result of the Lorentz Force. The maximum axial velocity decreases as the Hartmann number increases in order to maintain the same mass flux.

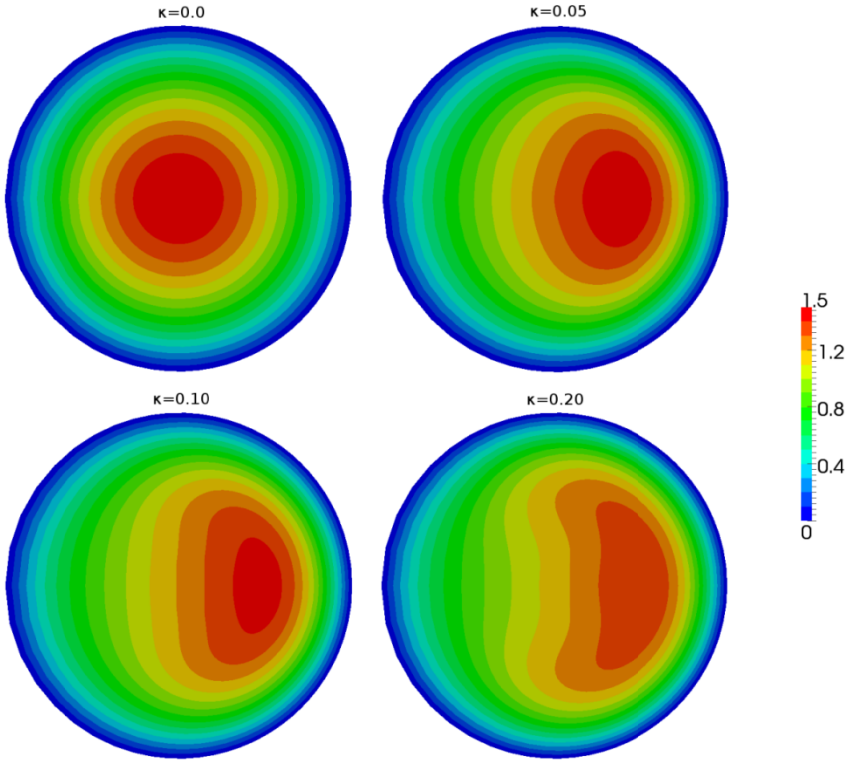

Figure 2. Contour plots of the axial velocity for *Ha* = 0 and various curvatures.

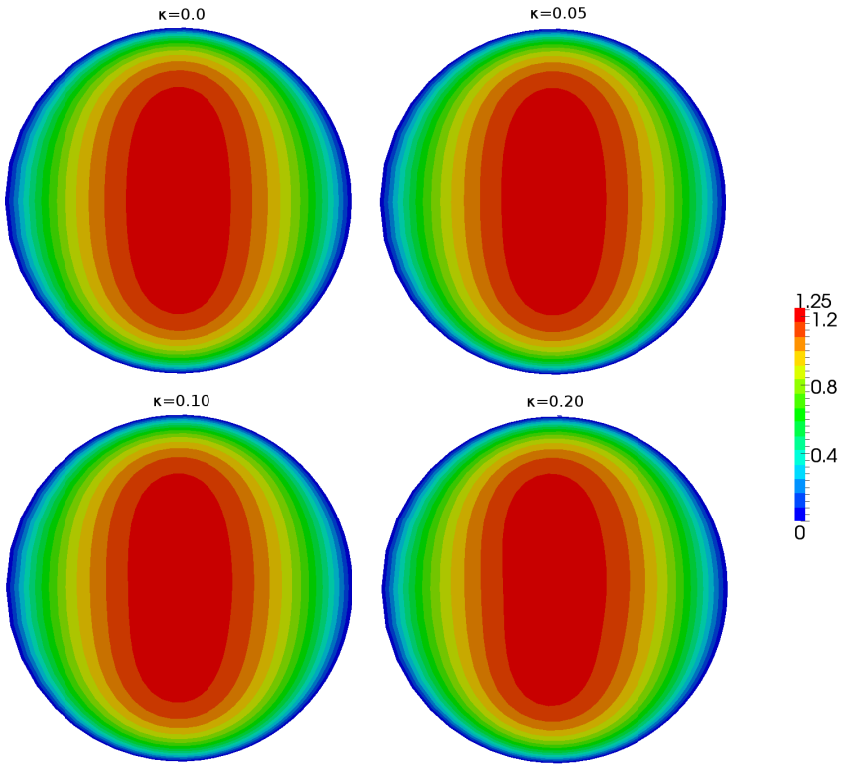

Figure 3. Contour plots of the axial velocity for *Ha* = 10 and various curvatures.

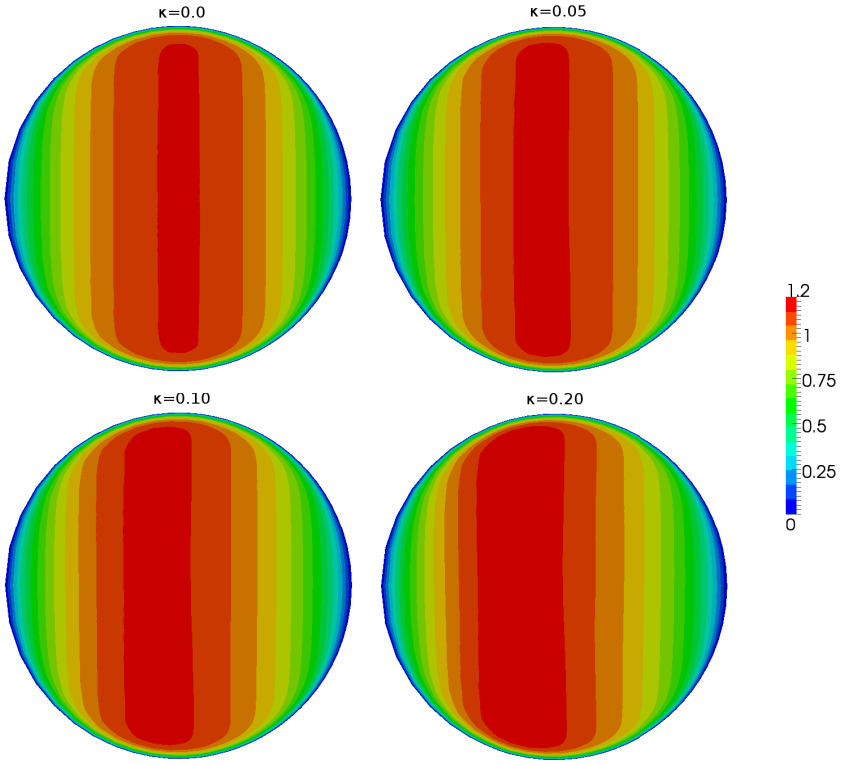

Figure 4. Contour plots of the axial velocity for *Ha* = 50 and various curvatures.

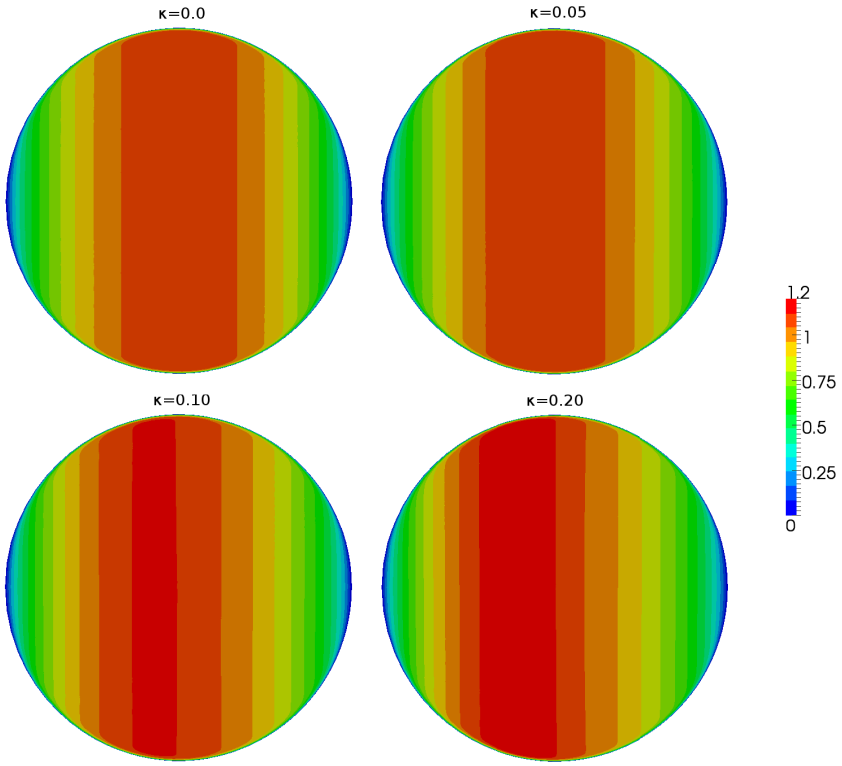

Figure 5. Contour plots of the axial velocity for *Ha* = 200 and various curvatures.

As the Hartmann number increases above 10, the electromagnetic force dominates and shifts the peak of the axial velocity to the left region of the cylinder as the curvature increases. In Figures 4 and 5 the distribution of the axial velocity is presented for *Ha* = 50 and *Ha* = 200 respectively and for κ = 0, 0.05, 0.10 and 0.20. In the case of the straight duct the peak of the velocity is located along the centerline of the pipe in a direction parallel to the external magnetic field. As the Hartmann number increases, the thin Hartmann boundary layers near the top and bottom sides of the cylinder rapidly decrease in thickness.

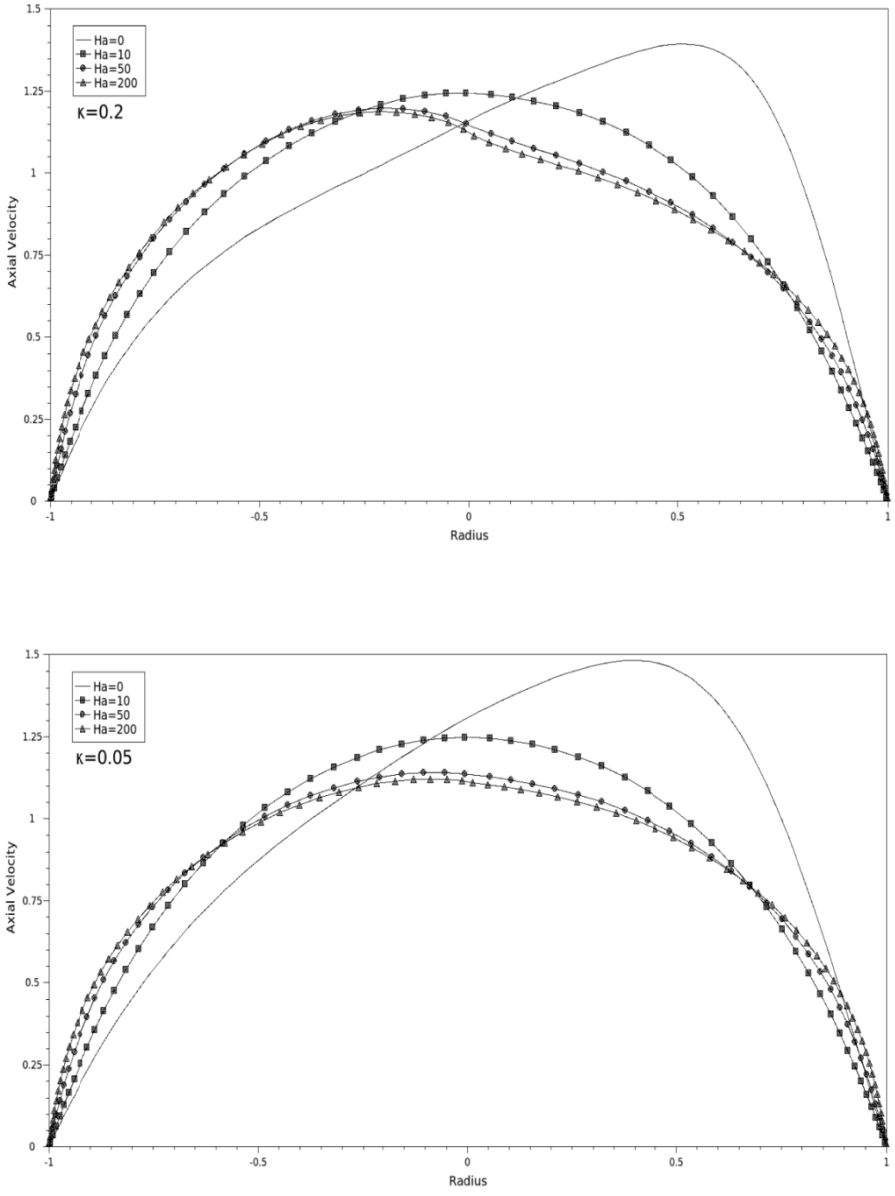

Figure 6. Axial velocity profile along the horizontal direction of the cylinder for κ = 0.2 and 0.05 and various Hartmann numbers.

The profile of the axial velocity along the horizontal direction of the cylinder for $\kappa = 0.2$ and 0.05 and various Hartmann numbers is presented in Figure 6. It can be observed that as the Hartmann number increases the axial velocity reduces more rapidly in the right region of the cylinder. As the Hartmann number increases above 50 the axial velocity profile slightly changes for both cases.

In Figure 7 the profile of the axial velocity is illustrated along the horizontal direction of the cylinder for $Ha = 0$ and 100 and various curvatures. The effect of the centrifugal forces and the shift of the velocity in the right region of the cylinder is clearly shown in the case of $Ha = 0$. For $Ha = 100$ it can be observed that the alteration of the axial velocity profile due to the increase of the curvature is smaller than in the case of $Ha = 0$.

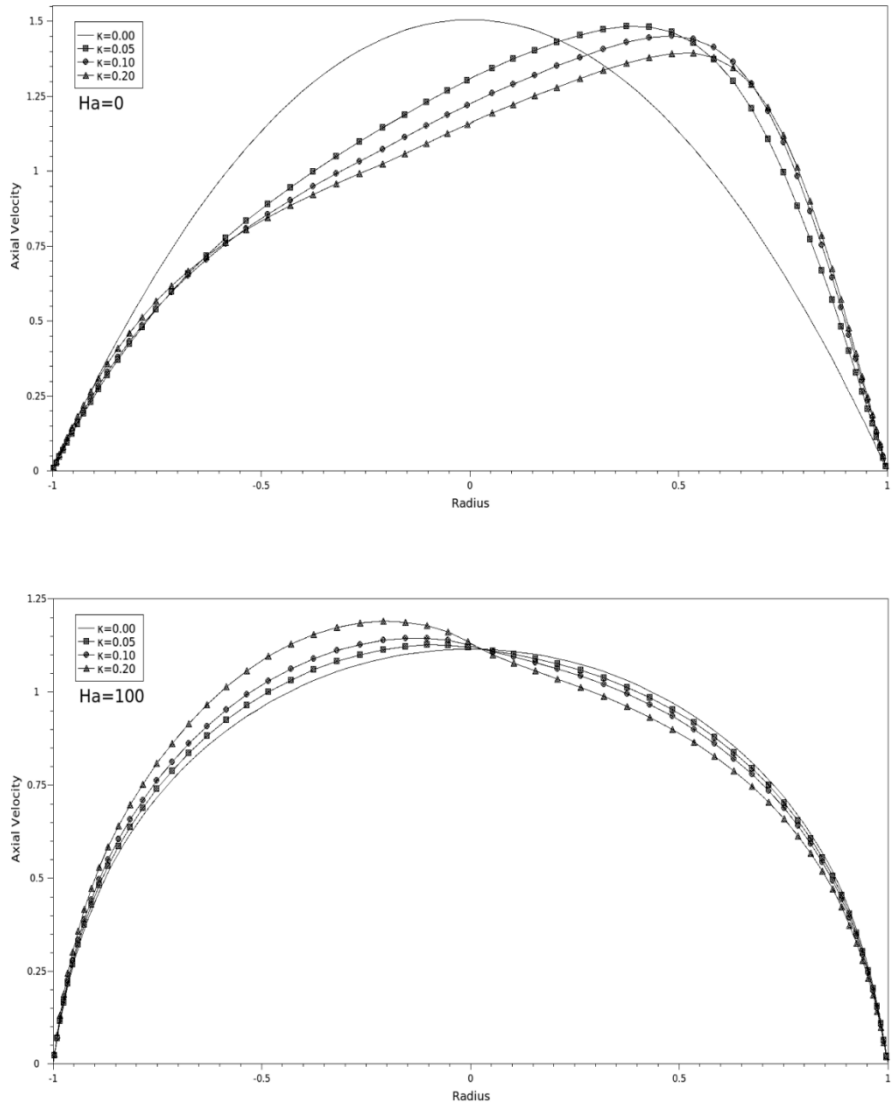

Figure 7. Axial velocity profile along the horizontal direction of the cylinder for $Ha = 0$ and 100 and various curvatures.

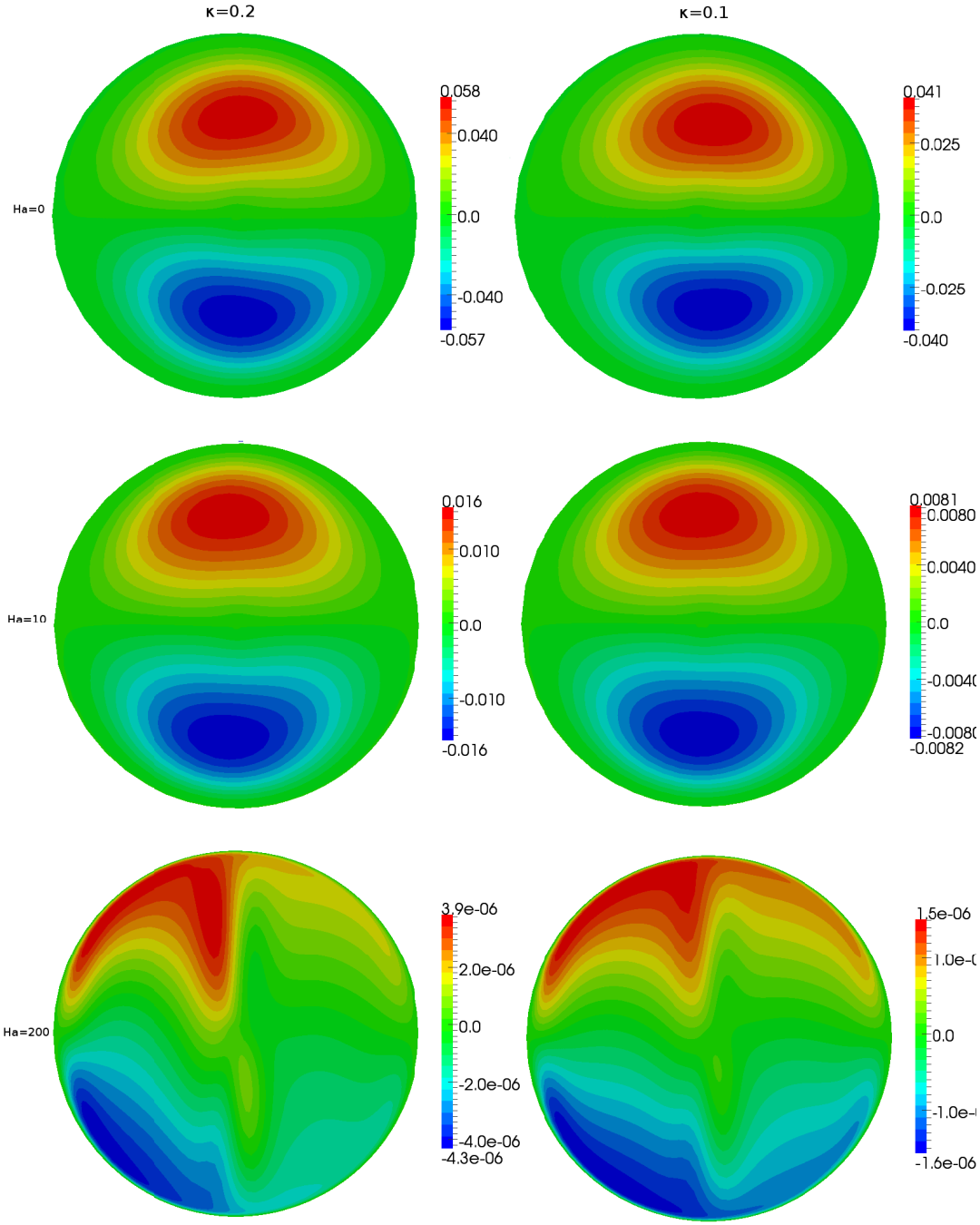

Figure 8. Contour plots of the streamlines of the transverse components of the velocity for Ha = 0, 10 and 200 and κ = 0.2 (left column) and 0.1 (right column).

The contour plots of the streamlines of the transverse components of the velocity are presented in Figure 8 for Ha = 0, 10 and 200 and κ = 0.2 and 0.1. The secondary flow is generated due to the effect of the curvature of the duct. Two circulation eddies are formulated, one clockwise (positive values) near the top of the cylinder and one anticlockwise (negative values) near the bottom of the cylinder. As the Hartmann number increases the secondary flow is strongly suppressed by the effect of the magnetic field. For Ha = 200 the secondary flow is negligible.

Ha	***Curvature κ***			
	0	**0.05**	**0.1**	**0.2**
0	-0.0601414798	-0.0701433519	-0.0801145549	-0.0934788329
10	-0.1395018848	-0.1396890427	-0.1401696893	-0.1419123240
50	-0.5761261148	-0.5786253173	-0.5806468819	-0.5832236343
100	-1.1245731957	-1.1298016526	-1.1339772109	-1.1391908283
200	-2.2229944556	-2.2335450986	-2.2421387084	-2.2528031702

Table 1. Axial pressure gradient p_{az} for various values of Hartmann number and curvature.

The pressure drop due to the effect of the curvature and the magnetic field is presented in Table 1. The contribution of the curvature in the axial pressure gradient is significant only in the case for Ha = 0, where for κ = 0.2 the axial pressure gradient is 55 per cent bigger than the one for κ = 0. The magnetic field significantly increases the axial pressure gradient by orders of magnitude.

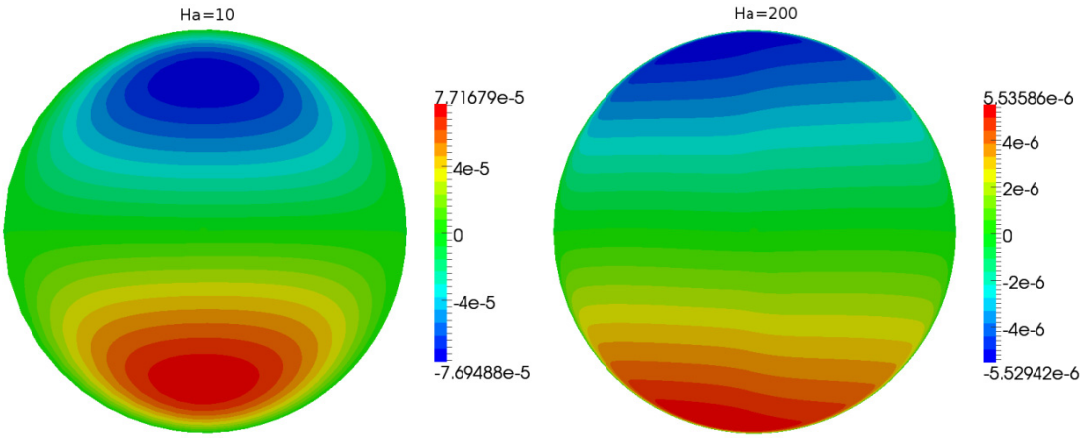

Figure 9. Contour plot of the induced axial magnetic field for Ha = 10 and 200 and κ = 0.1.

The distribution of the induced axial magnetic field is shown in Figure 9 for κ = 0.1 and for Ha = 10 and 200. It can be observed that the induced magnetic field is formulated into two regions, a positive region near the bottom of the cylinder and a negative region near the top of the cylinder. As the Hartmann number increases, these regions spread in the horizontal direction and the maximum absolute values of the induced magnetic field decrease. As a result of the small magnetic Reynolds number R_m the magnitude of the induced magnetic field is very small in comparison to the magnitude of the external magnetic field.

5 Conclusions

The effects of the curvature and the Hartmann number on the velocity distribution are presented in this paper. As the curvature increases the centrifugal force tends to shift the axial velocity to the right region of the cylinder and the electromagnetic force tend to shift the axial velocity to the left region of the cylinder. For Hartmann numbers lower than 10 the centrifugal force dominates and the axial velocity is shifted to the right region, while for Hartmann numbers greater than 10 the electromagnetic force dominates and the axial velocity is shifter to the left region of the cylinder. A secondary flow is generated due to the curvature of the duct. This secondary flow is strongly suppressed under the presence of an external magnetic field.

Acknowledgement

This work is part of "K. Karatheodoris 2009" program, funded by the University of Patras Research Committee.

References

[1] R. Kobayashi, "Stability of MHD Viscous Flow in a Curved Channel", Bulletin of the JSME, 20, 983-990, 1977.

[2] K. Sudou, Y. Tomita, R. Yamane, K. Ueda, S. Ohima, "Flow of Liquid Metals through Curved Circular Channels with a Transverse Magnetic Field", Bulletin of JSME, 27, 46-56, 1984.

[3] P. Tabeling, J. P. Chabrerie, "Magnetohydrodynamic Secondary Flows at High Hartmann numbers", Journal of Fluid Mechanics, 103, 225-239, 1981.

[4] F. Issacci, N. M. Ghoniem, I. Catton, "Magnetohydrodynamic Flow in a Curved Pipe", Physics of Fluids, 31, 65-71, 1988.

[5] A. Sterl, "Numerical simulation of liquid–metal MHD flows in rectangular ducts", Journal of Fluid Mechanics, 216, 161–191, 1990.

[6] S. Smolentsev, N. B. Morley, M. Abdou, R. Munipalli and R. Moreau, "Current approaches to modeling MHD flows in the dual coolant lead lithium blanket", Magnetohydrodynamics, 42 (2/3), 225-236, 2006.

[7] P.M. Hatzikonstantinou, V.D. Sakalis, “A numerical-variational procedure for laminar flow in curved square ducts”, International Journal for Numerical Methods in Fluids, 45 (12), 1269-1289, 2004.
[8] P.K. Papadopoulos, P.M. Hatzikonstantinou, “Improved CVP scheme for laminar incompressible flows”, International Journal for Numerical Methods in Fluids, 65 (9), 1115-1132, 2010.
[9] P.A. Bakalis, P.M. Hatzikonstantinou, “MHD and thermal flow between isothermal vertical concentric cylinders with rotation of the inner cylinder”, Numerical Heat Transfer, 59 (11), 836-856, 2011.
[10] P.A. Bakalis, P.M. Hatzikonstantinou, P. Vafeas, “Magnetohydrodynamic flow of a liquid metal between vertical isothermal rotating cylinders”, Proceedings of the 4th International Conference on Experiments, Process, System Modeling, Simulation, Optimization, vol. II, pp. 351–357, Athens, Greece, 2011.
[11] N. B. Morley, S. Smolentsev, R. Munipalli, M.-J. Ni, D. Gao. M. Abdou, “Progress on the Modelling of Liquid Metal, Free Surface, MHD Flows for Fusion Liquid Walls”, Fusion Engineering and Design, 72, 3-34, 2004.